Small-molecule modulators of the ATPase VCP/p97 affect specific p97 cellular functions

Figuerola Conchas, Ainoa; Saarbach, Jacques; Daguer, Jean Pierre; Cieren, Adeline; Barluenga Badiola, Sofia; Winssinger, Nicolas; Gotta, Monica

How to cite

FIGUEROLA CONCHAS, Ainoa et al. Small-molecule modulators of the ATPase VCP/p97 affect specific p97 cellular functions. In: ACS Chemical Biology, 2020, vol. 15, n° 1, p. 243–253. doi: 10.1021/acschembio.9b00832

This publication URL: https://archive-ouverte.unige.ch/unige:129089

Publication DOI: 10.1021/acschembio.9b00832

Small-molecule modulators of the ATPase VCP/p97 affect specific p97 cellular functions

Ainoa Figuerola-Conchas,[†, ‡, ¶] Jacques Saarbach,[‡, §, ¶] Jean-Pierre Daguer,[‡, §] Adeline Cieren,[†, ‡,] Sofia Barluenga,[‡, §] Nicolas Winssinger,*[,‡, §] Monica Gotta*[,†, ‡]

† Department of Cell Physiology and Metabolism, University of Geneva, 1211 Geneva 4, Switzerland

‡ Swiss National Centre for Competence in Research in Chemical Biology, University of Geneva, Geneva, Switzerland

§ Department of Organic Chemistry, University of Geneva, 1211 Geneva 4, Switzerland

ABSTRACT: VCP/p97 belongs to the AAA+ ATPase family and has an essential role in several cellular processes ranging from cell division to protein homeostasis. Compounds targeting p97 inhibit the main ATPase domain and cause cell death. Here, using PNA-encoded chemical libraries, we have identified two small molecules that target the regulatory domain of p97, comprising the N-terminal and the D1 ATPase domains, and do not cause cell death. One molecule, **NW1028**, inhibits the degradation of a p97-dependent reporter, whereas the other, **NW1030**, increases it. ATPase assays show that **NW1028** and **NW1030** do not affect the main catalytic domain of p97. Mapping of the binding site using a photo-affinity conjugate points to a cleft at the interface of the N-terminal and the D1 ATPase domains. We have therefore discovered two new compounds that bind to the regulatory domain of p97 and modulate specific p97 cellular functions. Using these compounds, we have revealed a role for p97 in the regulation of mitotic spindle orientation in HeLa cells.

INTRODUCTION

VCP/p97/Cdc48 is a member of the AAA$^+$ ATPase family type II which is ubiquitously expressed in multicellular organisms. P97 was initially identified in a screen for cell division cycle mutants in yeast.[1] However multiple other functions have emerged over the years, ranging from the most characterized one, binding to ubiquitylated protein and facilitating their degradation, to vesicle fusion, endocytosis, endolysosomal sorting and signaling.[2-7] The molecular activity of p97 is ATP driven unfolding, assisted by a wide range of adaptors, which account for the diversity of functions.[8-10] The energy released from the ATP hydrolysis is used to segregate client proteins from membranes or from protein complexes to be recycled or sent to degradation.

p97 is a homohexamer that forms a ring with a central pore (Figure 1A).[11] Each protomer is formed by an N-terminal domain followed by two ATPase domains in tandem, named D1 and D2 (Figure 1A). Both ATPase domains contain a Walker A and a Walker B motif that confer the ability to bind and hydrolyze ATP, with the D2 domain having higher ATPase activity. The N-terminal domain mediates the interaction with the adaptor proteins and the D1 ATPase domain is a regulatory domain that controls the conformation of the N-terminal domain in a nucleotide dependent-manner and promotes the formation of the hexamer.[12-14] The high ATPase activity of the D2 domain is required to achieve the main function of p97, aimed at performing a mechanical force to unfold proteins.[8, 9]

Several inhibitors of the D2 ATPase domain of p97 are available.[15-21] The most used p97 inhibitors identified recently, DBeQ, NMS-873 and MSC1094308[16, 19, 20] were isolated by screening compounds that inhibit the ATPase activity *in vitro*. Since p97 participates in a wide range of cellular processes, treatment with these drugs cause major cellular defects, including cell death. The cytotoxicity of these compounds has been exploited as a potential cancer therapy, bringing compounds such as CB-5083 (a DBeQ analogue) to clinical trials.[22, 23] Recent results have shown off-target activity highlighting the need of new more selective compounds to pursue this strategy.[24] Identification of modulators that target the regulatory domain of p97 may provide a tool to dissect the multiple functions of p97 by only targeting a subset.

Given the weak ATPase activity of the D1 domain and the lack of established ligands that could be used in a displacement assay, screening for D1 modulators by traditional high throughput screening is challenging. DNA-encoded libraries have emerged as a powerful technology enabling screens to be performed based on affinity selection without the need of a substrate or ligand for displacement.[25, 26] We have focused on PNA-(Peptidic Nucleic Acid)-encoded libraries based on

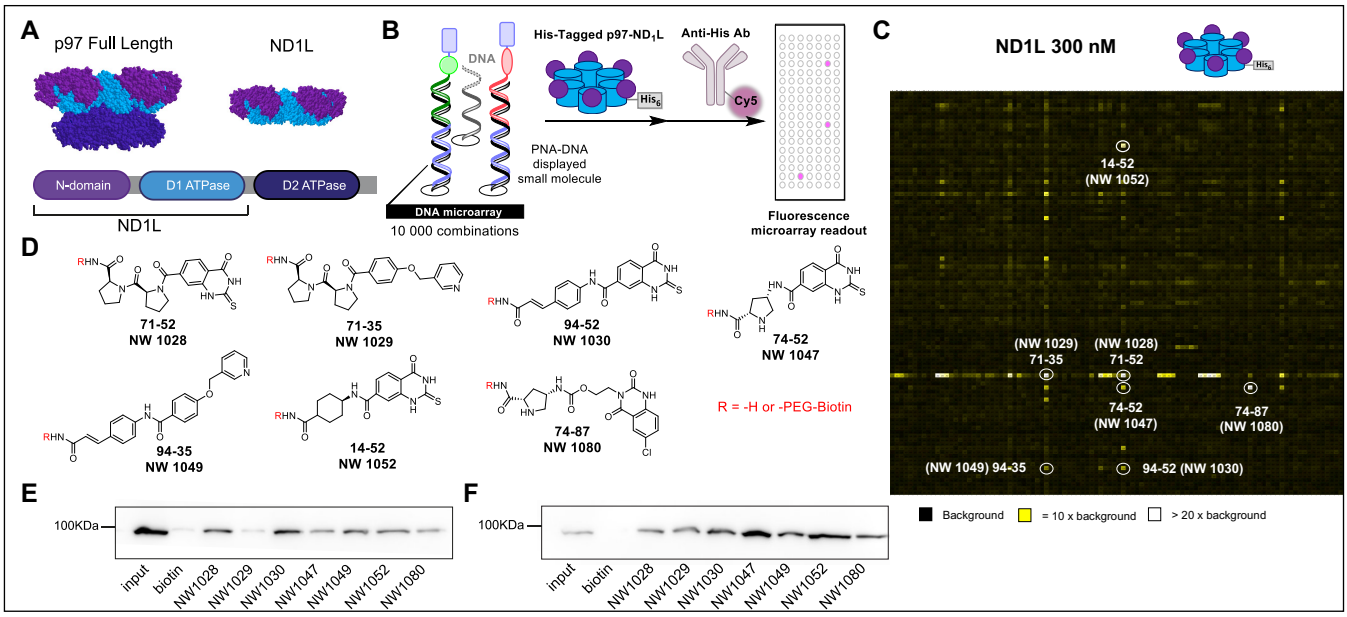

Figure 1: Identification of seven compounds that interact with the ND1L domain of p97. (A) Top: 3D structure of p97 full length (left) and the ND1L fragment (right) (pdb 5ftk); bottom: schematic representation of the p97domains using the same colour code as in the 3D structure. (B) Screening procedure; helices represent the DNA-PNA molecules with the attached chemical compounds. (C) Heat map of fluorescence intensity (Cy5 channel) for the screen of a 10 000 membered DNA-PNA encoded library against his tagged ND1L fragment revealed with an anti-His Ab-Cy5 conjugate. The Cy5 fluorescence is quantified and represented on 100 x 100 heat map with codon 1 on horizontal axis and codon 2 on vertical axis. The fluorescence intensities are the median of 4 values. Selected compounds are circled with the codon combination and assigned compound number in brackets. (D) Chemical structure of selected compounds resynthesised off-oligo and as biotin conjugates for hit validation. (E) and (F) pull-down of p97 from HEK 293 crude cell extracts with the different compounds without (E) and with ADP (F); Western-Blot performed with anti-p97 monoclonal antibody.

traditional solid phase peptide synthesis (SPPS).[27] PNA-encoded libraries can be hybridized and paired onto DNA templates (DNA display) for affinity-based selection or microarray-based screens.[28, 29] Optimal fragment pairs can be used for the synthesis of focused libraries.[29, 30] Using this technology, we focused our screen on binders targeting the regulatory domains of p97, the N-terminal domain and the D1 ATPase domain (ND1L, Figure 1B).

Here we present two new chemical compounds that are able to modulate p97 activity and affect a subset of its functions in cells. These compounds are not cytotoxic and allow cells to proliferate, making it possible to investigate the mitotic functions of p97. We show here that when cells are treated with these compounds, they display spindle orientation defects, demonstrating that p97 is required for this process.

RESULTS AND DISCUSSION

Affinity screen for chemical compounds that interact with the regulatory domains of p97. To identify compounds that modulate p97 without affecting the main ATPase function of D2, we performed an affinity screen using a recombinant fragment of p97 containing the N-terminal domain, the D1-ATPase domain and the D1-D2 linker (from here on referred to as ND1L). This fragment preserves the same hexamer configuration as the full length protein,31 but contains solely the regulatory domains of p97 (Figure 1A). Using existing fragment-based PNA-encoded chemical libraries,28-30 we identified ND1L binders from a focused library pairing in a covalent fashion 100 different natural and unnatural amino acids (each encoded with a unique 7mer PNA or codon 1) with 100 different fragments (each encoded with a unique 7mer PNA or codon 2) to obtain 10 000 unique PNA tagged compounds. The screen was performed by hybridizing the PNA-encoded library to a DNA microarray such that each compound hybridizes to a unique position on the array. Each DNA sequence is present four times on the array thus providing quality control through this redundancy. The array was incubated with the His-tagged ND1L, washed and subsequently incubated with a Cy-5 labelled anti-His Ab (Figure 1B). Scanning of the microarray revealed the best binders (Figure 1C). The fluorescence intensities are represented on 100 x 100 heat map with codons 1 as rows and codons 2 as columns. The fluorescence intensities are the median of 4 values. The same screen was performed in the presence of 2 mM ADP and 2 mM non-hydrolysable ATP (ATPγS) to interrogate the different conformations of ND1L and filter for ATP-competitive binders (Figure S1A and S1B). The fitness of a fragment in the library appears through horizontal or vertical lines (rows or columns) on the array. Analysis of the screen clearly revealed that row 71 followed by 74 gave the highest frequency of hits in combination with columns 35, 52 and 87 (Figure 1C). Seven com-

pounds representative of the different fragment combinations were selected for resynthesis and further validation in secondary screens (circled in Figure 1C and shown in Figure 1D).

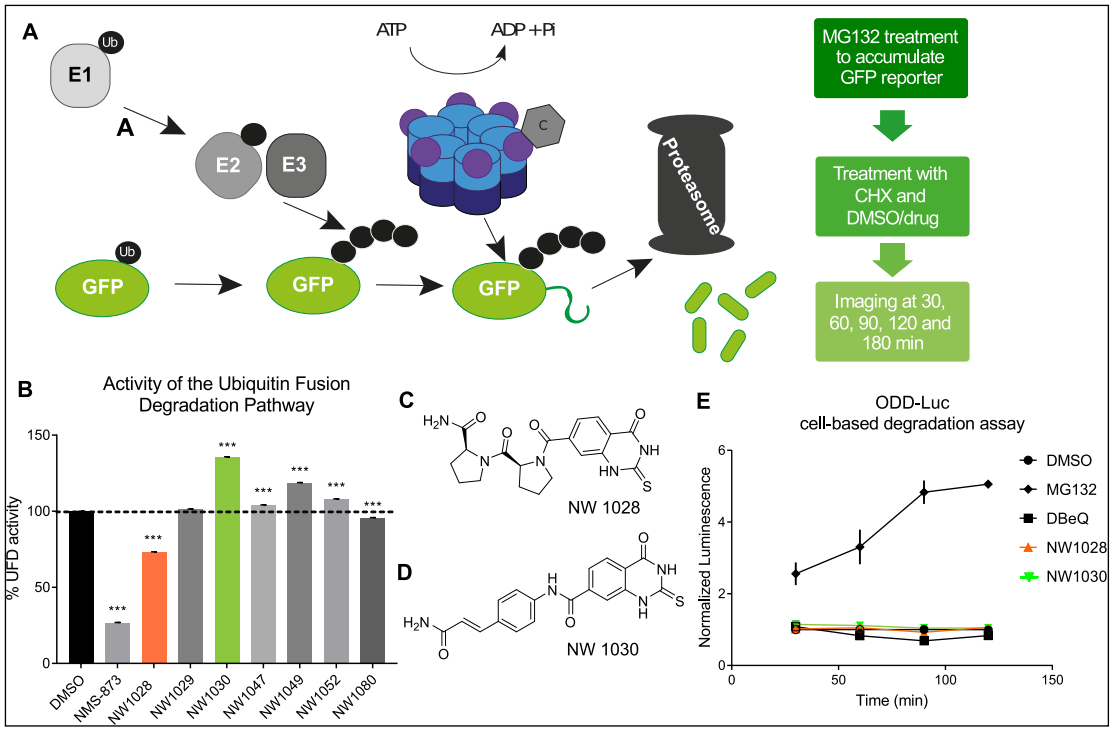

Figure 2: Activity of the compounds on a cell-based protein degradation assay. (A) Schematic representation of the cell-based protein degradation assay used to test the activity of the compounds. The UbG76V-GFP reporter is first stabilised for 1 h by treating cells with the proteasome inhibitor MG132; MG132 is then replaced by each compound (10 µM), DBeQ (10µM) as positive control or DMSO 0.1%, together with cycloheximide. (B) UFD pathway activity was assessed after stabilization of the UbG76V-GFP reporter prior treatment with the seven hits. The percentage of remaining UFD activity is calculated by the ratio between k_{deg}(compound)/k_{deg}(DMSO) (* indicate p < 0.001, Welch's test, Error bars correspond to SD; data correspond to three independent experiments, each performed with 3 replicas; in total between 1200 and 5600 cells were used to calculate the k_{deg}(compound)). (C) and (D) Structures of NW1028 and NW1030. (E) Accumulation of the p97 independent ODD-HIF1α-luciferase reporter over time: MG132 10µM, positive control, DBeQ 10µM, negative control, solvent alone, DMSO 0.1%, NW1028 and NW1030 10 µM. Error bars indicate SEM and the experiment was done three independent times.**

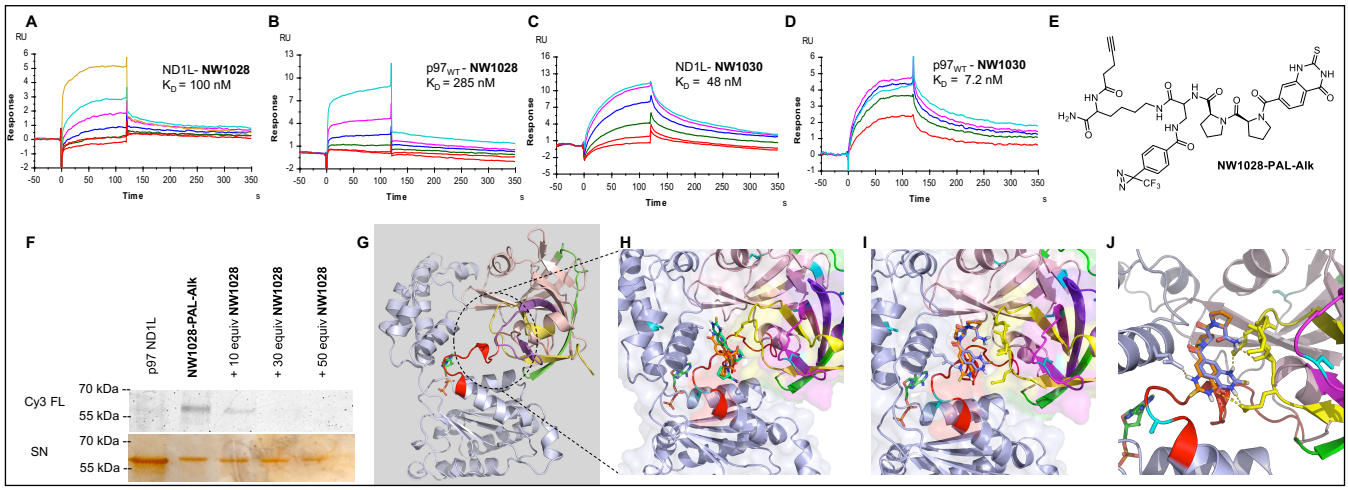

Figure 3: Affinity measurements and binding site studies. (A-D) SPR affinity measurements of NW 1028 on ND1L (A) and WT p97 (B) and of NW1030 on ND1L (C) and WT p97 (D). (E) Structure of the photoaffinity crosslinker derived from NW1028. (F) Photoaffinity labelling of ND1L by NW1028-PAL-Alk after click reaction. FL = Cy3 fluorescence and SN = Silver nitrate stain. (G) Peptides identified in the mass spectrometry experiments. Purple, yellow and red peptide = peptides with non reacted cysteines after treatment with iodoacetamide, green peptide = peptide identified by PAL. (H-J) Docking of NW1028 using autodock vina. (H) Conformation showing NW1028 with thiaquinazolinone moiety towards the upper part of the cleft. (I) Two different conformations showing NW1028 with

thiaquinazolinone moiety pointing down in the cleft. (J) Conformation found with the lowest energy, hydrogen bonds to the protein are displayed in yellow and orange.

Hit validation. First, compounds wherein the oligonucleotide tag was replaced by biotin (Figure 1D and table S4) were used in a pull-down assay. All the compounds were able to pull down p97 from HEK293 extracts, although to different extent in the presence or absence of ADP (Figure 1E and 1F).

To assess the activity of the compounds in cells, we monitored the function of p97 in the Ubiquitin-Fusion Degradation (UFD) pathway, taking advantage of a cell-based protein degradation assay.[32] For this purpose, the compounds were synthesized without a tag (Figure 1D and Supplementary Table S4). The assay consists of a dual reporter HeLa cell line stably expressing a UFD substrate: Ub^{G76V}-GFP, whose degradation depends on p97. We first stabilized the reporter by treating the cells with MG132, a proteasome inhibitor, and we subsequently added cycloheximide to inhibit protein synthesis together with the identified compounds (Figure 2A). The decay of GFP fluorescence was monitored over time and the rate of degradation k_{deg} was measured for each compound and compared to the DMSO control. We observed that the compounds affected significantly the degradation rate of the reporter (Figure 2B). The compounds **NW1030**, **NW1047**, **NW1049** and **NW1052** show a significant increase in the rate of decay of the reporter, compared to DMSO, whereas **NW1028** and **NW1080** decreased the rate of decay of the reporter (Figure 2B). From all compounds increasing the decay rate, **NW1030** was the most potent, whereas **NW1028** was the most potent in decreasing the decay rate (Figure 2B and Supplementary Figure S2 for detailed kinetics of degradation for **NW1028** and **NW1030**). We therefore selected **NW1028** and **NW1030** for further characterization (Figure 2C and 2D).

We next investigated the ability of **NW1028** and **NW1030** to modulate the degradation of p97-independent proteasome substrates, using a second reporter expressed in the same HeLa cell line, ODD-Luc (oxygen dependent degradation domain of HIF1α fused to luciferase).[32] Normalized luminescence values indicate that treatment with **NW1028** or **NW1030** does not affect the degradation of the reporter ODD-Luc, compared with the high increase of luminescence in presence of the proteasome inhibitor MG132 (Figure 2E).

We have identified two small molecules that bind to the ND1L domain of p97 and modulate the p97-dependent degradation of a reporter in cells: **NW1028**, which inhibits p97 function in protein degradation, and **NW1030** which increases this same activity.

To further characterize the interactions of the two selected compounds, we measured their binding affinity to p97 by Surface Plasmon Resonance (SPR). Initially, the protein hexamer was immobilized on a chip by NHS activation and the compounds injected on the protein. However, the hexamer was degraded during the regeneration step making this experimental design unsuitable for measurements and no reproducible data could be obtained (vide infra). To palliate this issue, the biotinylated version of the selected compounds was immobilized on a streptavidin biosensor (50RU) at a low density to limit avidity effects using the hexamer. Their affinity to ND1L fragment and WT p97 were measured using HBS buffer with 2 mM ADP. For **NW1028**, Kds of 100 nM (ND1L) and 285 nM (full length p97) were measured respectively, while for **NW1030**, Kds were of 48 nM (ND1L) and 7.2 nM (full length p97) (Figure 3 A-D). The binding affinity towards a walker B mutant of ND1L (ND1L E305Q), able to bind ATP but not hydrolyze it, was also measured and showed no change in K_D for any of the two compounds (see Supplementary Figure S3).

To gain insight into the binding site, we selected **NW1028** for photoaffinity labelling (PAL) studies. We modified the compound on the C-terminus based on the premise that this site must point towards the solvent to be identified in the PNA-encoded screen. The new compound (**NW1028-PAL-Alk**, Figure 3E) was prepared by SPPS starting the synthesis with a Lysine modified on one side with an alkyne for pulldown and the diazirine-based cross-linker on the other side (Supplementary Scheme S3). The compound was incubated with ND1L fragment and crosslinked by UV irradiation of the sample. The reaction was subsequently treated with an azide adduct bearing both a fluorophore (Cy3) for detection of labeling and desthiobiotin for pulldown. As shown in Figure 3F (and Supplementary Figure S5), in gel scanning in the Cy3 channel show a clear fluorescent band while the competition with 10 to 50 equivalents of unconjugated ligand (**NW1028**) showed reduced to no labeling, in agreement with the free ligand competing for the binding site on the protein. The same experiment was performed followed by a tryptic digest of the protein and the labeled protein fragments (peptides) were pulled down on a streptavidin resin. Elution of the fragments and MALDI analysis showed a single major peak at 3213.59 a.m.u. corresponding to the peptide segment 96-109 of ND1L (Supplementary Figure S6).

In separate experiments analyzing the digest of ND1L with or without ligand (**NW1028**) after reduction of cysteine and reaction with iodoacetamide, we observed a protection of cysteine reaction in the presence of the inhibitor on four peptides (segment 21-45, 65-81, 96-109, 191-211 of ND1L respectively in yellow, purple, green and red on Figure 3G, and Supplementary Table S2) adjacent to and including the peptide identified by pulldown. Collectively, these experiments point to a cleft between the D1 and the N-term domain as the binding site of **NW1028** (Figure 3G).

NW1028 was docked using autodock vina[33] on ND1. Using the reported crystal structure of ND1 in presence of

ADP (PDB: 5DYI)[13] was used and the docking space was limited to the cleft identified by mass spectroscopy studies. Two binding poses for **NW1028** were found based on the position of the quinazoline. Both poses can account for the mass spectrometry results observed (Figure 3H-3J, see Supplementary figure S7 for high resolution images). Docking of NW1030 using the same parameters gave two main poses (see Supplementary Figure S8), one of which the cinnamyl moiety is deeply buried in cavity formed by segment 21-45 of ND1 (in yellow).

NW1028 and NW1030 affect the activity of the D1 ATPase domain, but not the D2 domain. To investigate how the compounds could affect p97 functions, we performed ATPase assays using the p97 ND1L fragment (Figure 4A), which has weak yet measurable ATPase activity.[34] We performed the ATPase assays in presence of the **NW1028** and **NW1030** compounds.

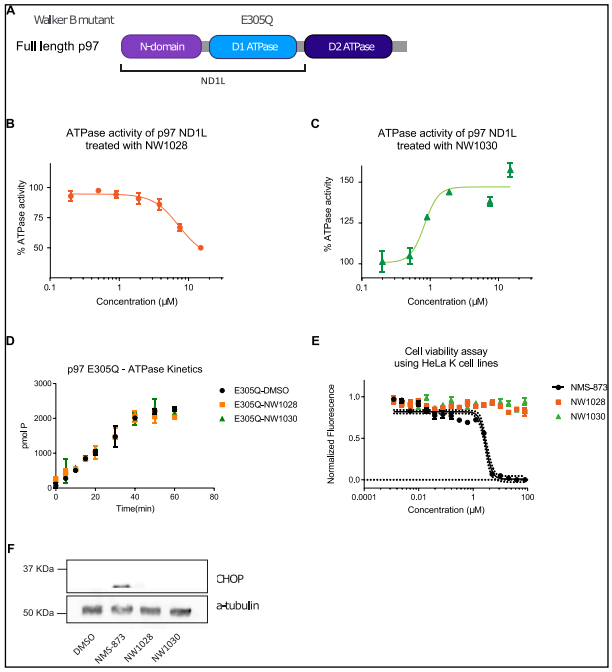

Figure 4: NW1028 and NW1030 affect specifically the D1 ATPase domain and do not cause cell death. (A) Schematic of p97 D2 walker B mutant able to bind but not hydrolyze ATP. (B) ATPase activity of p97 ND1L fragment measured using Malachite Green in the presence of different concentrations of NW1028 (400 nM p97-ND1L, two-fold dilutions starting with 15 μM of NW1028). (C) ATPase activity of p97 ND1L fragment measured using Malachite Green in the presence of different concentrations of NW1030 (400 nM p97-ND1L, two-fold dilutions starting with 15 μM of NW1030); (D) Kinetics of p97 E305Q ATPase activity measured using Malachite Green in the presence of NW1028 (500 nM p97-ND1L, 10 μM NW1028 or NW1030). The assays were done in three independent replicates. (E) Cell viability assays performed during 72h and analyzed using Preston Blue dye (see methods). Error bars correspond to SEM. Data were collected in three independent experiments. (F) Western Blot analysis of HeLa K cells treated with NMS-873 5μM, NW1028 10μM and NW1030 10μM for 8h. Data shown are representative results of one of three independent experiments.

The results show that treatment of ND1L with **NW1028** inhibits the ATPase activity of the D1 domain (Figure 4B), whereas **NW1030** increases the ATPase activity (Figure 4C). Known inhibitors of p97, such DBeQ and NMS-873, target the ATPase activity of the D2 domain.[16, 19] To assess whether **NW1028** and **NW1030** affect also the D2 domain of p97, we purified a recombinant p97 containing the mutation E305Q, which allows binding of ATP to the D1 ATPase domain, but not the

hydrolysis, allowing to monitor the D2 ATPase activity[34] (Figure 4A). Analysis of the ATPase assays show that **NW1028** and **NW1030** do not impact the ATPase activity of the D2 domain (Figure 4D). Incubation of cells with DBeQ and NMS-873 leads to the activation of the Unfolded Protein Response (UPR) and cell death.[16, 19] To assess whether treatment with **NW1028** and **NW1030** causes cell death, we performed cell viability assays. Incubation of HeLa K cells with NMS-873 for 72h caused cell death at an IC50 of 2.915 ± 0.186 μM (Figure 4E, mean ± SEM). Incubation with **NW1028** and **NW1030** (up to 80 μM) for 72h did not result in cell death (Figure 4E).

We subsequently asked whether these compounds were able to activate the UPR by monitoring the increase in the levels of CHOP (CCAAT-enhancer-binding protein homologous protein). CHOP is a proapoptotic factor downstream of the UPR and its expression is markedly increased upon prolonged ER-stress.[35] CHOP levels increased in cells treated with NMS-873, as previously reported[19], whereas they did not increase in cells treated with **NW1028** or **NW1030** (Figure 4F). In summary, **NW1028** and **NW1030** do not cause cell death and do not activate the UPR response. Additionally, **NW1028** and

NW1030 were tested in an 3-(4,5-dimethylthiazol-2-yl)-2,5-diphenyltetrazolium bromide (MTT) assay on HeLa cells and no cytotoxicity was observed up to 50 µM (Supplementary Figure S9). Altogether, the results indicate that we have identified small molecules affecting the D1 ATPase domain of p97, and not the D2, both in vitro and in cells.

NW1028 and NW1030 affect a subset of p97 functions in the cells. We subsequently asked if these small molecules can modulate other p97 dependent processes in cells. p97 is involved in a diverse array of functions in the cell, such as degradation associated with several organelles, autophagy or cilia formation.[5, 36, 37] p97 mutations lead to an accumulation of autophagosomes in patients with Inclusion Body Myopathy with early-onset Paget disease and Frontotemporal Dementia (IBMPFD).[38] Inhibition of p97 with DBeQ and NMS-873 also leads to a defect in autophagy and accumulation of autophagosomes.[16, 19] During autophagy, autophagosomes are formed as intermediate structures, which are converted in autolysosomes later on. Because autophagy is a dynamic pathway, an increase in the number of autophagosomes can correspond to an induction or an inhibition of autophagy. To distinguish between induction and inhibition of autophagy, we used a MEF cell line expressing a mCherry-GFP-LC3 reporter[38] (Figure 5A). This reporter exploits the difference between the two fluorescent proteins:

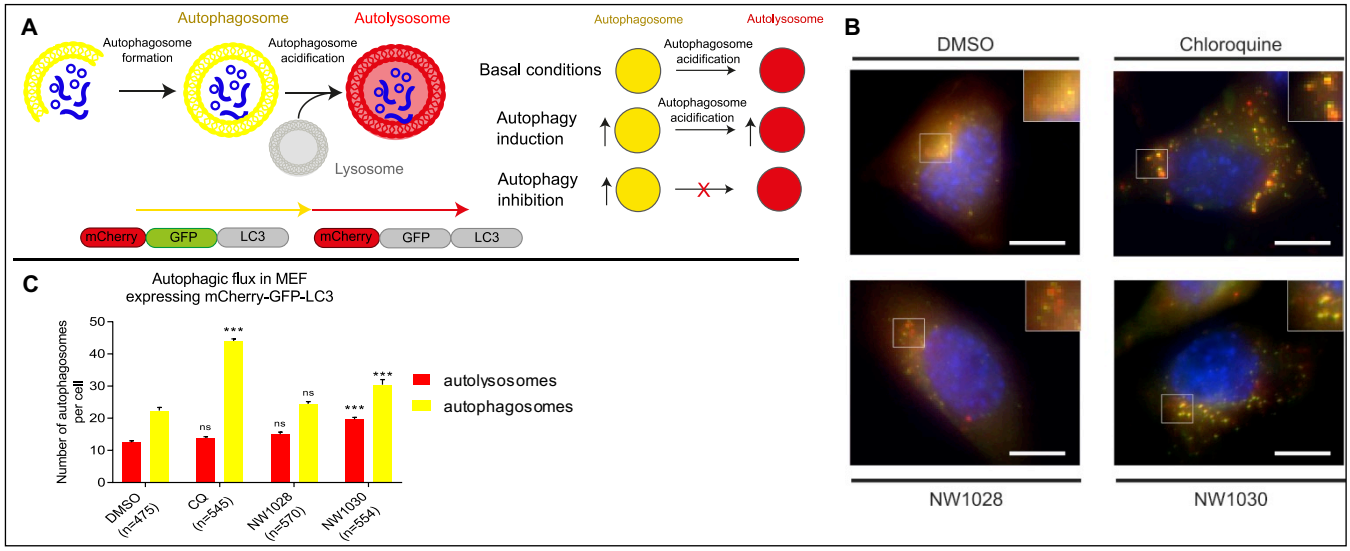

Figure 5: NW1030 increases the autophagic flux. (A) Schematic representation of the autophagic flux with the mCherry-GFP-LC3b reporter in which GFP is pH sensitive (left) and expected fluorescent outcome with this reporter when autophagy is inhibited or induced (right). (B) Representative example of fixed MEF cells (maximum intensity projections) expressing mCherry-GFP-LC3b after 3h treatment with 10 µM NW1028, 10 µM NW1030, 0.1% DMSO (negative control) or 10 µM chloroquine (positive control). (C) Quantification of number of autophagosomes and autolysosomes from (B) (* shows $p < 0.001$, ns indicates $p > 0.05$, 2-way ANOVA test) (Error bars indicate SEM). The measurements correspond to three independent experiments, n indicates the number of cells.**

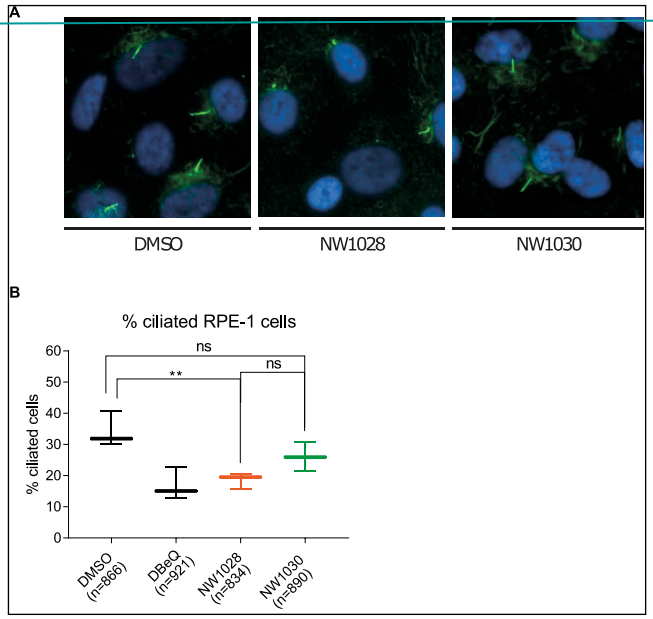

Figure 6: NW1028 affects cilia maintenance. (A) Representative images of RPE cells serum starved for 48h before treatment with DMSO (0.1%), NW1028 (10µM), NW1030 (10µM) and stained with an antibody recognizing acetylated tubulin (in green). DNA is stained with DAPI (Blue). (B) Quantification of the percentage of ciliated cells (* indicates $p < 0.05$, ns shows $p > 0.05$, Welch's test, Error bars correspond to SEM). DBeQ (10µM) is used as a positive control. Data were collected in triplicate, n indicates the number of cells.

GFP fluorescence is quenched in acidic compartments, while mCherry fluorescence is more stable in acidic conditions. It is therefore possible to distinguish between autophagosomes (GFP and mCherry fluorescence, i.e. "yellow autophagosomes") and autolysosomes (mCherry fluorescence, i.e. "red autolysosomes", Figure 5A). Induction of autophagy will cause an increase of yellow and red vesicles, whereas inhibition of autophagy will result in impairment of acidification and in an increase in yellow vesicles (Figure 5A). After treating the cells with chloroquine, an inhibitor of autophagy, we observed an increase of the number of vesicles LC3b positive for both mCherry and GFP ("yellow autophagosomes", Figure 5B and 5C, see Supplementary Figure S11 for high resolution image). Treatment with NW1028 did not cause a significant change in LC3b levels compared to control conditions (Figure 5B and 5C, Supplementary Figure S11). Incubation with **NW1030** caused an induction of autophagy, shown by the increase in the number of red and yellow autophagosomes (Figure 5B and 5C, Supplementary Figure S11). Altogether, we conclude that **NW1028** does not affect autophagy, whereas **NW1030** causes an increase of the autophagic flux.

P97, together with its adaptor protein UBXN-10, regulates primary cilia formation and maintenance.[37] We asked whether these compounds also have an effect on cilia maintenance. Primary cilia formation was induced by starving RPE cells and cilia were identified by immunostaining for acetylated tubulin. In control conditions, 34.3% of cells are ciliated (Figure 6A). After three hours of drug treatment, NW1028 reduced the number of

ciliated cells to 18.6% similar to the result obtained by treating the cells with DBeQ (Figure 6B). On the contrary, there was no significant difference in the number of ciliated cells when **NW1030** was used (Figure 6B).

These results further support the different effect of **NW1028** and **NW1030** in modulating p97 functions.

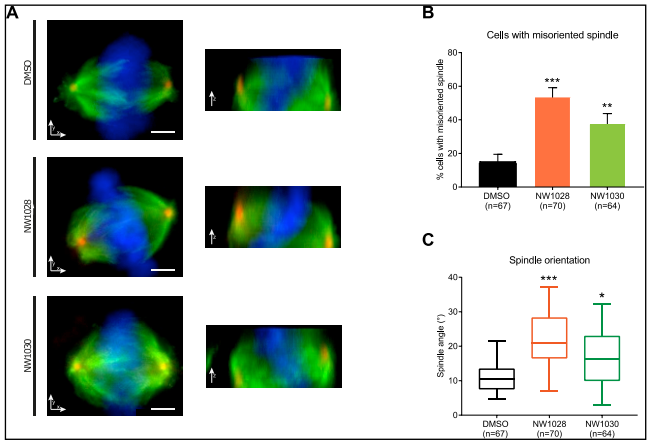

Figure 7: NW1028 and NW1030 affect the orientation of the mitotic spindle. (A) Images of HeLa cells treated with NW1028 and NW1030, fixed and immunostained with α-tubulin (green), γ-tubulin (red) antibodies and DAPI to visualise DNA (blue). Left panels: views from the *xy* axis; right panels: views from *z* axis. (B) Quantification of the number of cells with a spindle orientation defect (* indicate p < 0.001, ** p<0.01, Welch's test, Error bars show SEM). (C) Quantifications of spindle angles ((* shows p<0.05, *** indicate p < 0.001, Welch's test). The results correspond to three independent experiments, n indicates the number of cells.**

We then investigated whether **NW1028** and **NW1030** affect mitotic entry. We treated HeLa K cells expressing α-tubulin fused to GFP and H2B fused to mCherry and performed time-lapse microscopy. Whereas DBeQ treatment impaired mitotic entry and caused cell death[16] (movie 1), cells incubated with **NW1028** and **NW1030** entered mitosis, indicating that these two compounds do not impair mitotic progression or mitotic timing (movies 2, 3, DMSO control movie 4, Supplementary Figure S12). We noticed that when cells are incubated with **NW1028** and **NW1030**, the mitotic spindle oscillated from prometaphase until anaphase onset (movie 2, 3, DMSO control movie 4), a phenotype similar to the one observed when cells are depleted of the p97 adaptors p37 and p47.[39, 40] To quantify the spindle orientation phenotype, we measured the angle of the spindle at metaphase in fixed cells immunostained with γ-tubulin as a marker for the spindle poles. Consistent with the time-lapse observations, we detected that 53.9% of cells treated with **NW1028** and 37.7% of cells treated with **NW1030** had a spindle orientation defect in the *z* axis, compared to 14.9% cells in control conditions (Figure 7A and 7B). The mitotic spindle of non-treated cells is parallel to the substrate (10.7°±0.65, mean ± SEM), whereas in cells treated with **NW1028** the angle was 21.3°±1.55 and in cells treated with **NW1030** was 16.7°±1.72 (Figure 7C).

In brief, treatment of cells with **NW1028** or **NW1030** affects a subset of p97 dependent process but does not impair mitotic progression neither cause cell death. This allowed us to reveal the spindle orientation defect.

Here, we have used the regulatory domains of p97 to identify compounds that modulate p97 functions.

Interestingly, among the 7 hits selected from the primary screen, 5 compounds activate p97 function in the UFD pathway, whereas two inhibit the degradation rate. We have selected **NW1028**, the most potent inhibitor of degradation, and **NW1030** because of its potent effect in increasing the degradation rate of the UFD pathway. It is interesting to note that the two compounds share a common half of the structure (Figure 1D), but they show different activities. However, those activities are not always opposite. For instance, autophagic flux is not affected by **NW1028** whereas treatment with **NW1030** causes an increase of the flux. Both compounds inhibit cilia maintenance although only treatment with **NW1028** has a significant effect. Also, both compounds lead to spindle orientation defects during mitosis in HeLa cells, demonstrating that p97 regulates spindle orientation. These results suggest that both activation and inhibition of p97 can lead to the same defects in cells (e.g. spindle orientation defects). Alternatively, the drugs may selectively affect the interaction with adaptors (see below).

Inhibition of p97 using DBeQ or NMS-873 causes major cellular defects and cell death.[16, 19] **NW1028** and **NW1030** are not cytotoxic and **NW1028** diminishes the ATPase activity of the D1 domain whereas **NW1030** increases this activity, but neither of the two compounds alter the activity of the D2 domain (Figure 4). These results suggest that in cells **NW1028** and **NW1030** do not affect the main activity of p97, but rather modulate it, either by affecting the binding of p97 with some of its adaptor proteins or by affecting the conformation of the D1 domain.

Perturbing the function of a target protein with a small molecule rather than through a genetic approach or antisense approach has the advantage of simpler temporal regulation. This can be crucial to study targets necessary for cell viability. The results presented herein highlight another asset of a small molecule approach: the ability to perturb a subset of the functions of a multifunctional protein complex. This was enabled by an affinity screen for the regulatory domains of p97 (ND1L) yielding compounds that do not interact with the main function of p97 (D2 domain). DNA or PNA-encoded libraries facilitate the biochemical characterization by providing synthetically tractable handle for biotin or photoaffinity conjugates.

METHODS

Materials. Antibodies used in this study are: anti-α-tubulin, anti- α-acetyl-tubulin and γ-tubulin (Sigma-Aldrich), anti-p97 (Fitzgerald 1ORP104A), anti-CHOP (Cell Signalling Technology), Alexa Fluor 568 goat anti-mouse and Alexa Fluor 488 goat anti-rabbit (Invitrogen), Goat Anti-Rabbit IgG Horseradish Peroxidase conjugate and Goat Anti-Mouse IgG Horseradish Peroxidase conjugate (GE-healthcare), Protease inhibitor cocktail (Roche) PhosphoStop (Roche), Phosphatase inhibitor (Roche) streptavidin coated magnetic beads DynalTm (Invitrogen, Life Technologies), nitrocellulose membranes (Macherey Nagel), ECL Prime Western Blotting Detection (GE Healthcare), PXi/PXi Touch luminescence detector (Syngene), Pierce high capacity Streptavidin Agarose beads (Thermofisher), Trypsin singles, proteomic grade (Sigma-Aldrich), 96-well clear-bottom black plate (Falcon), 96-well white plates (Greiner Bio-One)

Chemicals used in this study are: MG132 and DBeQ (Sigma-Aldrich), NMS-873 (Xcessbio), chloroquine (Enzo lifescience), cycloheximide (Millipore), puromycin (Sigma-Aldrich), G418 (InvivoGen) and luciferin (AppliChem).

Cell culture and transfections. The following cell lines were gifts from specified groups: HeLa cells expressing UbG76V-GFP and ODD-LUC, gift of T. Chou 16 (Harbor-UCLA Medical Center and Los Angeles Biomedical Research Institute, USA); HEK 293T, RPE1, HeLa, HeLa H2B-mCherry/GFP-α-tubulin41 from P. Meraldi (University of Geneva, Switzerland); MEF cells expressing mCherry-GFP-LC3b, from P. Taylor (Tresse et al., 2010) (St. Jude Children's Research Hospital, USA).

Cell lines were grown in Dulbecco's modified eagle medium (Gibco DMEM) supplemented with FCS 10%, penicillin 100units/ml and streptomycin 100mg/ml) at 37°C with 5% CO2 in a humified incubator. HEK 293T cells were supplemented with 1% Glutamine. HeLa cells expressing UbG76V-GFP and ODD-LUC were selected with 2.5µg/ml puromycin and

0.1mg/ml G418(Chou and Deshaies, 2011). Transient expression was performed using lipofectamine 2000 (Invitrogen) according to the manufacturer's protocol.

Plasmids and oligonucleotides. The following constructs were used in this work for protein expression and site-directed mutagenesis: pQE9-His-p97deltaD2 was provided by Addgene (ID17229); pET15-His-p97 and pET24b-His-p97ND1L was provided by TF. Chou 34 (Harbor-UCLA Medical Center and Los Angeles Biomedical Research Institute, USA).

The mutant p97 E305Q were obtained by site-directed mutagenesis using the following oligonucleotides: p97 E305Q (forward: GCCATCATCTTCATTGAT CAGCTAGATGCCATCGCTCCC; reverse: GGGAGCGATGGCATCTAGCTGATCAATGAAGATGATGGC). The following oligonucleotides were used to verify the site-directed mutagenesis: ATGGCTTCTGGAGCCGATTC, TTACCCGATGTCTTCCCAGGTTAC, GTAACCTGGGAAGACATCGGG, GGAACAGGTAGCCAATGAGACTC and GGCCATCCGTGAATCCATCG.

Recombinant protein expression and purification. All recombinant proteins (ND1L and p97 E305Q) were expressed in E.coli BL21 (Rosetta) containing the desired plasmid. Bacterial cultures were grown with shaking at 37°C to an OD600nm of 0.5 in 2XTY medium (16 g tryptone, 10 g yeast extract and 5 g NaCl in 1 L deionised water) containing the antibiotics to select each plasmid (chloramphenicol 20 µg/ml and either carbenicilin 100 µg/ml or kanamycine 50 µg/ml). Induction was performed at 22°C with 0.8 mM IPTG overnight.

Bacteria were harvested and the pellet was resuspended in lysis buffer (100 mM Tris, pH 7.4, 500 mM KCl, 5 mM MgCl2, 5% glycerol, 2 mM β-mercaptoethanol and a protease inhibitor cocktail). The cells were lysed by sonication in three 60-seconds pulses on ice. The lysate was centrifuged at 10000 rpm at 4°C for 20 minutes. The supernatant was loaded onto a TALON Resin column containing the equilibration buffer (50 mM HEPES pH 7.4, 150 mM KCl, 5 mM MgCl2). The column was washed with washing buffer (equilibration buffer containing 20 mM imidazole) and His-tag proteins were eluted by adding increasing concentrations of elution buffer (equilibration buffer containing 25, 50, 100, 200 and 300 mM imidazole). The fractions containing the proteins were pooled together. Imidazole was removed by dialysis with the assay buffer (50 mM HEPES pH 7.4, 150 mM KCl, 5 mM MgCl2).

Screening of the heterocycle library was performed on an Agilent microarray where the 10000 DNA sequences complementary to the 10000 membered heterocycles PNA encoded library had been spotted. Each sequence in this Agilent design is spotted four times. (Agilent array design 041896).

PNA encoded libraries were hybridised on the microarray at an equimolar concentration of 5 µM (total concentration of library, 0.5 nM of individual library members), overnight at 50°C, in PBS-Tween 0.1% buffer, 40 % formamide. The slide was subsequently washed twice with PBS-Tween 0.1% and once with Milli-Q water to remove excess of library and non-specific hybridizations.

Recombinant his tagged-ND1L protein expressed on E. coli was diluted to 300 nM in selection buffer, 200 mM HEPES pH 7.4, 0.5 M KCl, 50 mM MgCl2, 0.01% Tween20, 5 mM β-Mercapto-ethanol.

His tagged-ND1L was incubated with the hybridised PNA library for two hours at room temperature with gentle rotation. After two hours incubation, the hybridisation chamber was dismounted and the array slide was washed with selection buffer and once with Milli-Q water just before being dried by centrifugation (5 min at 1000 g).

The slide was placed again on the hybridisation chamber and stained with anti-His DyLight 649 coupled antibody (Rockland Immunogenics). The antibody was incubated 20 min (diluted 1/5000 in PBS-Tween 0.1%, 0.5% BSA) and the washing procedure and drying of the slide were repeated as described above. Finally, the slide was scanned at 635 nm on a Genepix Personnal Scanner.

Preparation of crude cell extracts. HEK293T were washed with cold, sterile PBS and finally scraped in 1 ml of cold lysis buffer (50 mM Tris-HCl pH 8, 150 mM KCl, 5 mM MgCl2, 5 % glycerol, 1% Triton X100, 2 mM β-mercaptoethanol, 1X phosphostop and 1X protease inhibitors). The protein lysate was centrifuged for 30 min at 14000 rpm, to eliminate cell membranes and cell debris. The supernatant was transferred to a fresh tube, and the soluble cytosolic proteins were quantified by Bradford.

Affinity based capture of proteins from crude cell extracts. 10 µL of streptavidin coated magnetic beads DynalTm, were washed three times with the buffer (50 mM Tris-HCl pH 8, 150 mM KCl, 5 mM MgCl2, 5% glycerol, 1% Triton X100, 2 mM β-mercaptoethanol) and resuspended in a solution of 100 µM biotinylated small molecule compounds and incubated for 15 minutes with gentle rotation. The functionalised beads were then washed twice with the buffer above and incubate with 50 µg of crude cell extract on the rotation wheel for another 30 min period, to allow small molecule protein interaction. Then the beads were washed 3 times with 100 µl of buffer and re-suspended with 1X SDS Sample buffer. The retained proteins were loaded and separated on 10% SDS PAGE electrophoresis. This method was adapted from previous protocols.42

After transfer to nitrocellulose membranes, the membranes were blocked (5% non -fat dry milk in PBS-Tween 0.1%) and incubated with anti-p97 monoclonal antibody diluted 1/1000 in 5% dry milk, followed by three washes with PBS-Tween.

The membranes were incubated with HRP conjugated antibodies and washed prior imaging. Proteins were detected using ECL Prime Western Blotting Detection and a PXi/PXi Touch luminescence detector.

Western Blot. Cells were washed in ice-cold PBS and resuspended in lysis buffer (50mM Tris pH 8, 150mM KCl, 5mM MgCl2, 5% glycerol, 1% triton X-100, 2mM β-Mercaptoethanol, protease inhibitor and phosphatase inhibitor. The lysate was incubated in ice for 30min and cleared by centrifugation at 10000 rpm for 10min at 4°C. 20µg of cell extract was resolved by SDS-PAGE and transferred to a nitrocellulose membrane (Whatman). Membranes were blocked with 5% dried milk in PBS 0.2% Tween 20, followed by overnight incubation with the primary antibodies listed on the table above. Secondary HRP-conjugate antibodies also listed above were incubate for 45min at room temperature. Proteins were detected by chemiluminescence.

Quantitative cell-based degradation assay. HeLa UbG76V-GFP;ODD-Luc were seeded in a 96-well clear-bottom black plate for the fluorescence assay or 96-well white plates for luminescence assay. After 16 h, cells were treated for 1 h with MG132 4 µM in Leibovitz L-15 media for 1 h. The medium was replaced by fresh L-15 containing DMSO 0.1% or testing compounds 10 µM, and CHX 30 µg/ml. Image acquisition was performed on an ImageXpress XL automatic microscope (Molecular Devices) at 30, 60, 120 and 180min with 20X objective to assess fluorescence. To measure luminescence, the same procedure was followed, except that at each time point D-Luciferin (50µl of 1 mg/ml) was added and luminescence signal measured in a plate reader SpectraMax Paradigm (Molecular Devices). GFP average intensity per cell was quantified using MetaXpress software. The background (non-treated cells) was subtracted from the mean intensity for each condition. The degradation constant was obtained from the slope of the linear regression after plotting natural logarithm (Ln) of the mean intensity versus the time.

Surface plasmon resonance mesurements. Biotinylated compounds were immobilized on SA chip (50 RU) following Biacore recommendations. Recombinant P97ND1L or the corresponding mutant protein, were in-jected in HBS-T 50 mM KCl-5 mM MgCl2. Serial dilutions of protein were done to 1 µM, 0.5 µM, 0.25 µM, 0.125 µM, 0.0625 µM and 0.031 µM, and the buffer was eventually complemented with 2 mM ADP for each concentration. Flow was set at 30 µL/min, contact time on association step was 120 s and on dissociation step was also 120 s. KD was determined using the thermodynamic equilibrium method from BiaEvaluation software and experiments were carried out as triplicates.

Crosslinking experiments. A 100 µL solution of 18 µM of ND1L and 10 µM of NW1028-PAL-Alk was prepared in buffer (50 mM HEPES pH 7.4, 150 mM KCl, 5 mM MgCl2). The solution was shaken on ice (or at 4°C) for an hour. The mixture was irradiated 3 min on ice by UV light (350 - 450 nm, 1000 W).

Click reaction. Stock solutions were prepared as follow. DTB Cy3 linker 1.25 mM in DMSO, TCEP 14 mg/mL in water, TBTA 1.6 mM in tBuOH/DMSO 2/8, CuSO4 50 mM in water. For 100 µL of protein, a solution of 2 µL of TCEP, 4 µL of DTB-Cy3, 2 µL of CuSO4 and 6 µL of TBTA was prepared. The mixture was vortexed for 30s and added to the protein solution. The reaction was shaken at 25°C for 45 min to maximum 1 h and stopped by protein precipitation.

Protein precipitation. For 100 µL of protein at 18 µM, were added the following solvent, kept ice cold, 470 µL methanol + 118 µL chloroform + 350 µL water. The heterogeneous solution was centrifuged 10 min at 20 000g at 4°C. After centrifugation a pellet formed at the interphase between the two layers. The aqueous/alcoholic as well as the chloroform layer were sequentially discarded without removing the pellet. The pellet was air dried and could be used in following steps.

Tryptic digest of proteins. The protein precipitate was suspended in 300 µL 50 mM ammonium bicarbonate pH 8.0. The protein was solubilized by sonication on ice (10 short pulses). To each sample was added 1 µg trypsin. The sample was shaken overnight at 600 rpm at 37°C. The following day, the reaction was stopped by addition of 10 µL of 1% formic acid in water.

Tryptic digest pulldown. 30 µL High capacity streptavidin agarose beads were used per sample. The beads were washed 3 times with 50 mM ammonium bicarbonate (beads were pelleted by centrifugation 1 min at 1500 rpm). The tryptic digest in acidified ammonium bicarbonate was added to the beads and the beads were agitated on a wheel at 25°C for 2 h. The beads were then washed with 2x 1% SDS, 4x mQ water or 2x PBS-T 0.05% and 2x mQ water. The beads were eluted using 5 mM biotin in 50 mM ammonium bicarbonate or by heating the beads to 95°C for 5 min two times in 100 µL mQ water. The sampled were analyzed immediately by MALDI, if more concentrated samples were needed the samples were lyophilized and solubilized in 30% acetonitrile + 0.1% formic acid in water.

Tryptic digest after cysteine modification. Prepare a fresh stock solutions of iodoacetamide 500 mM in 50 mM ammonium bicarbonate pH 8.0 buffer. Stock solution of TCEP 500 mM in ammonium bicarbonate can be stored at -20°C. ND1L (50 µL, 18 µM) was incubated with 100 µM of NW1028 or DMSO for 1h at 4°C. After this, the protein was treated with a solution of 5 mM TCEP and 5 mM Iodoacetamide. The reaction was shaken 30 minutes at 25°C protected from light. 1 µg of trypsin was dissolved in 500 µL ammonium bicarbonate 50 mM pH 8.0 and 250 µL of this solution were added to each sample. The protein was digested overnight at 37°C. The reaction was quenched by addition of 1/10 volume of 10% TFA, pH should be <2. The sampled were desalted using microspin desalting columns.

ATPase activity measures. Enzymatic activity measures were performed according to previously described protocols (Rowlands et al., 2004).

Malachite green reagent was prepared as follow: malachite green (Acros AC611255000) (0.0812%, w/v), polyvinyl alcohol (2.32%, w/v), ammonium molybdate (5.72%, w/v, in 6 M HCl), and mQ water,mixed in a 2:1:1:2 ratio.

ATPase activity EC50 measurement: Recombinant p97-ND1L-His was diluted to 500 nM in ATPase assay buffer, (50 mM Tris–HCl pH 7.4, 20 mM MgCl2 and 0.01% Triton X-100). Stock solutions of compounds, NW1028 or NW1030, were prepared at 150 µM, 75 µM, 37.5 µM, 18.7 µM, 9.37 µM, 4.6 µM, 2.34 µM, 1.1 µM to 0.58 µM by serial dilutions. For each compound concentration, 20 µL of compound stock solution was added to 160 µL solution of 500 nM ND1L-his in assay buffer. The enzyme –compound mixture was incubated at room temperature for 15 min. The reaction was started by addition of 20 µL of 1 mM ATP to the previous reaction mixture (protein + small molecule) and then incubated for 1 h at 37°C. 50 µL aliquots were transferred to a 96 well plate and 30 µL of freshly prepared malachite green reagent were added. After 1 min, the reaction was stopped by addition of 34% sodium citrate (10 µL). The 630 nm absorbance of the plate was measured on a Spectramax M5 spectrophotometer (Molecular Devices) and the values obtained were corrected by background subtraction. The data was plotted and fitted using PrismGraph software. Final concentration of ND1L was 400 nM and 0.1 mM of ATP, compound concentration ranged from 15 µM to 0.058 µM.

ATPase kinetics measurement: Recombinant His-p97 E305Q was diluted to 500 nM in ATPase assay buffer. To this solution (500 µL) was added 1 µL of 100 µM NW1028 / NW1030 or the corresponding volume of DMSO as control reaction (dilution is considered to be negligible). The small molecule enzyme mixture was incubated at room temperature for 15 min. Then the reactions were incubated at 37°C and 5 µL of 100 mM ATP was added to the reaction at t=0 min (start of hydrolysis) and 50 µL aliquots taken out from the reaction mix at 5, 10, 15, 20, 30, 40, 50 and 60 min and transferred in a 96-well plate. To each time point 30 µL of malachite green reagent was added. After 1 min, the reaction was stopped by addition of 34% sodium citrate (10 µL). Absorbance was measured at 630 nm and data analyzed as described in the EC50 assay. Final concentration of protein is considered to be 500 nM, 10 µM of compound and 1 mM of ATP.

Autophagosome quantification: To quantify autophagic flux a MEF cell line expressing a mCherry-GFP-LC3{Tresse, 2010 #31} reporter was used. Cells were treated with NW1028 and NW1030 (10 µM for 3 hours) and fixed with paraformaldehyde. Chloroquine was used as a positive control. Puncta were quantified automatically using the Spot detection function of the Imaris software.

Cilia formation. Primary cilia were induced by starvation. RPE cells were grown to 80% confluency followed by starvation with DMEM, without serum for 48h. Drugs to test or DMSO was added during 3h (10µM or 0.1%, respectively) and cells were fixed adding PFA 4% for 15min. Immunostaining was performed as explained above using anti-α-acetylated-tubulin.

Spindle orientation measurement. Spindle orientation was measured by taking the distance between the centrosomes (identified by γ-tubulin immunostaining) in metaphase and the z-sections of 0.5µm for each cell and calculating the angle compared to the substrate using the Pythagoras theorem (Figure S6B).

Image acquisition. Time-lapse imaging was performed at 37°C with Leibovitz L-15 medium containing 10% FCS in a Nikon Ti Wide-field microscope with a 60x oil objective. The recordings were performed every 3min during 12h as three-dimensional stacks. The immunofluorescence was done in the same microscope also with a 60x oil objective and as three-dimensional stacks. All images were quantified using FIJI software.

Statistical analyses. Paired two-tailed t tests, one-way ANOVA tests, Welch's test, Mann-Whitney tests, and Kruskal-Wallis tests were calculated on PRISM (7.02; GraphPad Software). Graphs were plotted in PRISM and mounted in Illustrator.

ASSOCIATED CONTENT

Supplementary figures and synthetic procedures as well as analysis of the synthesized compounds can be found in the supporting information. This material is available free of charge via the Internet at http://pubs.acs.org.
Raw data associated with experiments has been deposited and is available (www.zenodo.org).
Accession Codes
Raw data associated with experiments has been deposited and
is available http://doi.org/10.5281/zenodo.3539008

AUTHOR INFORMATION

Corresponding Authors

* Monica Gotta, E-mail: monica.gotta@unige.ch
Nicolas Winssinger, E-mail: Nicolas.winssinger@unige.ch

Author Contributions

A.F.C, J.S, JP.D., A.C., S.B., N.W. and M.G. conceived and designed experiments as well as analysed the data. JP. D. performed the screen using PNA-encoded chemical libraries. J.S. synthesised the molecules and validated hits with JP.D., S.B., A.F.C and A. C.. A.F.C. performed the cell biology assays with support from A.C., designed the constructs and purified the recombinant proteins. A.F.C. and S.B. coordinated the project activities. The figures were prepared by A.F.C., J.S., S. B., N. W. and M.G.

¶ These authors contributed equally.

Funding Sources

Work in the Gotta and the Winssinger laboratories are supported by the Swiss National Centre for Competence in Research in Chemical Biology (NCCR Chemical Biology), by grants from the Swiss National Science Foundation, and by the University of Geneva.

Notes

The authors declare no competing interests

ACKNOWLEDGMENT

Authors are grateful to P. Meraldi (University of Geneva, Geneva, Switzerland), M. Chanson (University of Geneva, Geneva, Switzerland) and R. Loewith (University of Geneva, Geneva, Switzerland) for discussions, TF. Chou (Harbor-UCLA Medical Center and Los Angeles Biomedical Research Institute, USA), and P. Taylor (St. Jude Children's Research Hospital, USA) for reagents, M. Prouteau, C. Bourgoint and F. Schwager (University of Geneva, Geneva, Switzerland) for support in protein purification, the Bioimaging platform of the Medical Faculty of the University of Geneva for microscopy support, the members of the Gotta and Meraldi groups for the discussions, and Françoise Schwager for technical support.

ABBREVIATIONS

FL, Fluorescence, Cy3, Cyanine 3, DMSO, Dimethylsulofxide, IPTG, MG, malachite green, PAL, Photoaffinity labelling, PNA, Peptide Nucleic Acid. ND1L, p97 ND1L fragment, SPPS, solid phase peptide synthesis, TBTA, Tris[(1-benzyl-1H-1,2,3-triazol-4-yl)methyl]amine, DTB, desthiobiotin, DMEM, Dubelco's minimum essential medium, SN, silver stain, TCEP, Tris(2-carboxyethyl)phosphine hydrochloride, IPTG, Isopropyl β-D-1-thiogalactopyranoside, UPR, unfolded protein response

REFERENCES

1. Moir, D., Stewart, S. E., Osmond, B. C., and Botstein, D. (1982) Cold-Sensitive Cell-Division-Cycle Mutants of Yeast - Isolation, Properties, and Pseudo-Reversion Studies, *Genetics 100*, 547-563.

2. Johnson, E. S., Ma, P. C. M., Ota, I. M., and Varshavsky, A. (1995) A Proteolytic Pathway That Recognizes Ubiquitin as a Degradation Signal, *J Biol Chem 270*, 17442-17456.

3. Kondo, H., Rabouille, C., Newman, R., Levine, T. P., Pappin, D., Freemont, P., and Warren, G. (1997) p47 is a cofactor for p97-mediated membrane fusion, *Nature 388*, 75-78.

4. Li, J. M., Wu, H. Y., Zhang, W. Z., Blackburn, M. R., and Jin, J. P. (2014) The p97-UFD1L-NPL4 Protein Complex Mediates Cytokine-Induced I kappa B alpha Proteolysis, *Mol Cell Biol 34*, 335-347.

5. Meyer, H., Bug, M., and Bremer, S. (2012) Emerging functions of the VCP/p97 AAA-ATPase in the ubiquitin system, *Nat Cell Biol 14*, 117-123.

6. Ritz, D., Vuk, M., Kirchner, P., Bug, M., Schutz, S., Hayer, A., Bremer, S., Lusk, C., Baloh, R. H., Lee, H., Glatter, T., Gstaiger, M., Aebersold, R., Weihl, C. C., and Meyer, H. (2011) Endolysosomal sorting of ubiquitylated caveolin-1 is regulated by VCP and UBXD1 and impaired by VCP disease mutations, *Nat Cell Biol 13*, 1116-U1148.

7. Uchiyama, K., Jokitalo, E., Kano, F., Murata, M., Zhang, X. D., Canas, B., Newman, R., Rabouille, C., Pappin, D., Freemont, P., and Kondo, H. (2002) VCIP135, a novel essential factor for p97/p47-mediated membrane fusion, is required for Golgi and ER assembly in vivo, *J Cell Biol 159*, 855-866.

8. Blythe, E. E., Olson, K. C., Chau, V., and Deshaies, R. J. (2017) Ubiquitin- and ATP-dependent unfoldase activity of P97/VCP center dot NPLOC4 center dot UFD1L is enhanced by a mutation that causes multisystem proteinopathy, *P Natl Acad Sci USA 114*, E4380-E4388.

9. Bodnar, N. O., and Rapoport, T. A. (2017) Molecular Mechanism of Substrate Processing by the Cdc48 ATPase Complex, *Cell 169*, 722-735.

10. Buchberger, A., Schindelin, H., and Hanzelmann, P. (2015) Control of p97 function by cofactor binding, *Febs Lett 589*, 2578-2589.

11. Tang, W. K., and Xia, D. (2016) Role of the D1-D2 Linker of Human VCP/p97 in the Asymmetry and ATPase Activity of the D1-domain, *Sci Rep-Uk 6*.

12. Jentsch, S., and Rumpf, S. (2007) Cdc48 (p97): a 'molecular gearbox' in the ubiquitin pathway?, *Trends Biochem Sci 32*, 6-11.

13. Tang, W. K., Li, D. Y., Li, C. C., Esser, L., Dai, R. M., Guo, L. A., and Xia, D. (2010) A novel ATP-dependent conformation in p97 N-D1 fragment revealed by crystal structures of disease-related mutants, *Embo J 29*, 2217-2229.

14. Wang, Q., Song, C. C., and Li, C. C. H. (2003) Hexamerization of p97-VCP is promoted by ATP binding to the D1 domain and required for ATPase and biological activities, *Biochem Bioph Res Co 300*, 253-260.

15. Chapman, E., Maksim, N., de la Cruz, F., and La Clair, J. J. (2015) Inhibitors of the AAA+ Chaperone p97, *Molecules 20*, 3027-3049.

16. Chou, T. F., Brown, S. J., Minond, D., Nordin, B. E., Li, K. L., Jones, A. C., Chase, P., Porubsky, P. R., Stoltz, B. M., Schoenen, F. J., Patricelli, M. P., Hodder, P., Rosen, H., and Deshaies, R. J. (2011) Reversible inhibitor of p97, DBeQ, impairs both ubiquitin-dependent and autophagic protein clearance pathways, *P Natl Acad Sci USA 108*, 4834-4839.

17. Ding, R., Zhang, T., Wilson, D. J., Xie, J. S., Williams, J., Xu, Y., Ye, Y. H., and Chen, L. Q. (2019) Discovery of Irreversible p97 Inhibitors, *J Med Chem 62*, 2814-2829.

18. Fang, C. J., Gui, L., Zhang, X., Moen, D. R., Li, K., Frankowski, K. J., Lin, H. J., Schoenen, F. J., and Chou, T. F. (2015) Evaluating p97 inhibitor analogues for their domain selectivity and potency against the p97-p47 complex, *ChemMedChem 10*, 52-56.

19. Magnaghi, P., D'Alessio, R., Valsasina, B., Avanzi, N., Rizzi, S., Asa, D., Gasparri, F., Cozzi, L., Cucchi, U., Orrenius, C., Polucci, P., Ballinari, D., Perrera, C., Leone, A., Cervi, G., Casale, E., Xiao, Y., Wong, C., Anderson, D. J., Galvani, A., Donati, D., O'Brien, T., Jackson, P. K., and Isacchi, A. (2013) Covalent and allosteric inhibitors of the ATPase VCP/p97 induce cancer cell death, *Nat Chem Biol 9*, 548-U544.

20. Pohler, R., Krahn, J. H., van den Boom, J., Dobrynin, G., Kaschani, F., Eggenweiler, H. M., Zenke, F. T., Kaiser, M., and Meyer, H. (2018) A Non-Competitive Inhibitor of VCP/p97 and VPS4 Reveals Conserved Allosteric Circuits in Type I and II AAA ATPases, *Angew Chem Int Edit 57*, 1576-1580.

21. Zhou, H. J., Wang, J. H., Yao, B., Wong, S., Djakovic, S., Kumar, B., Rice, J., Valle, E., Soriano, F., Menon, M. K., Madriaga, A., von Soly, S. K., Kumar, A., Parlati, F., Yakes, F. M., Shawver, L., Le Moigne, R., Anderson, D. J., Rolfe, M., and Wustrow, D. (2015) Discovery of a First-in-Class, Potent, Selective, and Orally Bioavailable Inhibitor of the p97 AAA ATPase (CB-5083), *J Med Chem 58*, 9480-9497.

22. Lan, B., Chai, S., Wang, P., and Wang, K. (2017) VCP/p97/Cdc48, A Linking of Protein Homeostasis and Cancer Therapy, *Curr Mol Med 17*, 608-618.

23. Vekaria, P. H., Home, T., Weir, S., Schoenen, F. J., and Rao, R. (2016) Targeting p97 to Disrupt Protein Homeostasis in Cancer, *Front Oncol 6*, 181.

24. Tang, W. K., Odzorig, T., Jin, W., and Xia, D. (2019) Structural Basis of p97 Inhibition by the Site-Selective Anticancer Compound CB-5083, *Mol Pharmacol 95*, 286-293.

25. Goodnow, R. A., Dumelin, C. E., and Keefe, A. D. (2017) DNA-encoded chemistry: enabling the deeper sampling of chemical space, *Nat Rev Drug Discov 16*, 131-147.

26. Neri, D., and Lerner, R. A. (2018) DNA-Encoded Chemical Libraries: A Selection System Based on Endowing Organic Compounds with Amplifiable Information, *Annu Rev Biochem 87*, 479-502.

27. Zambaldo, C., Barluenga, S., and Winssinger, N. (2015) PNA-encoded chemical libraries, *Curr Opin Chem Biol 26*, 8-15.

28. Daguer, J. P., Ciobanu, M., Alvarez, S., Barluenga, S., and Winssinger, N. (2011) DNA-templated combinatorial assembly of small molecule fragments amenable to selection/amplification cycles, *Chem Sci 2*, 625-632.

29. Daguer, J. P., Zambaldo, C., Abegg, D., Barluenga, S., Tallant, C., Muller, S., Adibekian, A., and Winssinger, N. (2015) Identification of Covalent Bromodomain Binders through DNA Display of Small Molecules, *Angew Chem Int Ed Engl 54*, 6057-6061.

30. Barluenga, S., Zambaldo, C., Ioannidou, H. A., Ciobanu, M., Morieux, P., Daguer, J. P., and Winssinger, N. (2016) Novel PTP1B inhibitors identified by DNA display of fragment pairs, *Bioorg Med Chem Lett 26*, 1080-1085.

31. Chia, W. S., Chia, D. X., Rao, F., Bar Nun, S., and Geifman Shochat, S. (2012) ATP binding to p97/VCP D1 domain regulates selective recruitment of adaptors to its proximal N-domain, *PLoS One 7*, e50490.

32. Chou, T. F., and Deshaies, R. J. (2011) Quantitative Cell-based Protein Degradation Assays to Identify and Classify Drugs That Target the Ubiquitin-Proteasome System, *J Biol Chem 286*, 16546-16554.

33. Trott, O., and Olson, A. J. (2010) AutoDock Vina: improving the speed and accuracy of docking with a new scoring function, efficient optimization, and multithreading, *J Comput Chem 31*, 455-461.

34. Chou, T. F., Bulfer, S. L., Weihi, C. C., Li, K. L., Lis, L. G., Walters, M. A., Schoenen, F. J., Lin, H. J., Deshaies, R. J., and Arkin, M. R. (2014) Specific Inhibition of p97/VCP ATPase and Kinetic Analysis Demonstrate Interaction between D1 and D2 ATPase Domains, *J Mol Biol 426*, 2886-2899.

35. Deshaies, R. J. (2014) Proteotoxic crisis, the ubiquitin-proteasome system, and cancer therapy, *Bmc Biol 12*.

36. Meyer, H., and Weihl, C. C. (2014) The VCP/p97 system at a glance: connecting cellular function to disease pathogenesis, J Cell Sci 127, 3877-3883.

37. Raman, M., Sergeev, M., Garnaas, M., Lydeard, J. R., Huttlin, E. L., Goessling, W., Shah, J. V., and Harper, J. W. (2015) Systematic proteomics of the VCP-UBXD adaptor network identifies a role for UBXN10 in regulating ciliogenesis, *Nat Cell Biol 17*, 1356-+.

38. Tresse, E., Salomons, F. A., Vesa, J., Bott, L. C., Kimonis, V., Yao, T. P., Dantuma, N. P., and Taylor, J. P. (2010) VCP/p97 is essential for maturation of ubiquitin-containing autophagosomes and this function is impaired by mutations that cause IBMPFD, *Autophagy 6*, 217-227.

39. Kress, E., Schwager, F., Holtackers, R., Seiler, J., Prodon, F., Zanin, E., Eiteneuer, A., Toya, M., Sugimoto, A., Meyer, H., Meraldi, P., and Gotta, M. (2013) The UBXN-2/p37/p47 adaptors of CDC-48/p97 regulate mitosis by limiting the centrosomal recruitment of Aurora A, *J Cell Biol 201*, 559-575.

40. Lee, B. H., Schwager, F., Meraldi, P., and Gotta, M. (2018) p37/UBXN2B regulates spindle orientation by limiting cortical NuMA recruitment via PP1/Repo-Man, *J Cell Biol 217*, 483-493.

41. McHedlishvili, N., Wieser, S., Holtackers, R., Mouysset, J., Belwal, M., Amaro, A. C., and Meraldi, P. (2012) Kinetochores accelerate centrosome separation to ensure faithful chromosome segregation, *J Cell Sci 125*, 906-918.

42. Fischer, J. J., Graebner, O. Y., Dalhoff, C., Michaelis, S., Schrey, A. K., Ungewiss, J., Andrich, K., Jeske, D., Kroll, F., Glinski, M., Sefkow, M., Dreger, M., and Koester, H. (2010) Comprehensive Identification of Staurosporine-Binding Kinases in the Hepatocyte Cell Line HepG2 using Capture Compound Mass Spectrometry (CCMS), *J Proteome Res 9*, 806-817.

Authors are required to submit a graphic entry for the Table of Contents (TOC) that, in conjunction with the manuscript title, should give the reader a representative idea of one of the following: A key structure, reaction, equation, concept, or theorem, etc., that is discussed in the manuscript. Consult the journal's Instructions for Authors for TOC graphic specifications.